Novelty-Sensitive Dopaminergic Neurons in the Human Substantia Nigra Predict Success of Declarative Memory Formation

Jan Kami ski[1,4,*], **Adam N. Mamelak**[1], **Kurtis Birch**[1], **Clayton P. Mosher**[1], **Michele Tagliati**[2], and **Ueli Rutishauser**[1,2,3,4,5,*]

[1]Department of Neurosurgery, Cedars-Sinai Medical Center, 8700 Beverly Boulevard, Los Angeles, CA 90048, USA

[2]Department of Neurology, Cedars-Sinai Medical Center, 8700 Beverly Boulevard, Los Angeles, CA 90048, USA

[3]Center for Neural Science and Medicine, Department of Biomedical Sciences, Cedars-Sinai Medical Center, 8700 Beverly Boulevard, Los Angeles, CA 90048, USA

[4]Computation and Neural Systems, Division of Biology and Biological Engineering, California Institute of Technology, 1200 E California Boulevard, Pasadena, CA91125, USA

Summary

The encoding of information into long-term declarative memory is facilitated by dopamine. This process depends on hippocampal novelty signals, but it remains unknown how midbrain dopaminergic neurons are modulated by declarative-memory-based information. We recorded individual substantia nigra (SN) neurons and cortical field potentials in human patients performing a recognition memory task. We found that 25% of SN neurons were modulated by stimulus novelty. Extracellular waveform shape and anatomical location indicated that these memory-selective neurons were putatively dopaminergic. The responses of memory-selective neurons appeared 527 ms after stimulus onset, changed after a single trial, and were indicative of recognition accuracy. SN neurons phase locked to frontal cortical theta-frequency oscillations, and the extent of this coordination predicted successful memory formation. These data reveal that dopaminergic neurons in the human SN are modulated by memory signals and demonstrate a progression of information flow in the hippocampal-basal ganglia-frontal cortex loop for memory encoding.

*Correspondence: jan.kaminski@cshs.org (J.K.), ueli.rutishauser@cshs.org (U.R.).
[5]Lead Contact

Introduction

The formation of declarative memories relies on the ability of hippocampal synapses to rapidly change their strength through long-term potentiation and depression [1]. The strength and duration of synaptic plasticity depends on extracellular dopa-mine levels [2, 3], a neuromodulator that is released in the hippocampus from axonal terminals projecting from dopaminergic neurons in the substantia nigra (SN) and ventral tegmental area (VTA) [4]. The strength of hippocampal declarative memories is modulated by dopamine release: both the extent of SN/VTA activation [5, 6] and levels of dopamine within the hippocampus [2, 7] modulate the success of encoding. When animals are exposed to new environments, dopamine levels rise and facilitate long-term potentiation in the hippocampus. This enhanced memory for novel environments, however, is lost when hippocampal dopamine receptors are blocked [8]. Although these and other observations suggest a critical role for dopamine released by SN/VTA neurons in declarative memory [9–11], the underlying mechanisms that regulate this response are poorly understood.

Studying how SN/VTA dopaminergic neurons signal reward and reward expectation errors [12–14] has revealed a mechanistic understanding of the role of the SN/VTA in classical conditioning and reinforcement learning [15]. In addition, in humans, SN neurons also respond to infrequent sounds in an odd-ball paradigm [16] and encode decision outcomes [17]. In contrast, little is known about the role of SN/VTA in the acquisition of declarative memories. Although SN dopaminergic neurons respond to novel stimuli during conditioning [13, 18–20], no recordings exist of SN neurons during declarative memory tasks. It therefore remains unknown whether SN neurons differentiate familiar from novel stimuli and whether such activation is related to memory encoding success.

It has been proposed that the dopaminergic system and the hippocampus form a multisynaptic loop that starts with a hippocampal novelty signal that transiently excites dopaminergic neurons in the SN/VTA, which in turn leads to strengthening of hippocampal plasticity through the activation of hippocampal dopamine receptors (Figure 1A) [9, 23]. Although the original hypothesis concerns both the SN and the VTA, our focus here is only on the SN, and we thus restrict the following discussion to predictions relevant to the SN. Also, we do not limit the discussion to dopaminergic SN neurons, because GABAergic neurons in turn inhibit dopaminergic (DA) neurons [24], making their response equally relevant to the hypothesis. The hippocampus-SN/VTA loop hypothesis [9, 23] makes three specific predictions with respect to declarative memories: first, it predicts that the activity of SN neurons is modulated by stimulus novelty during declarative memory tasks. Second, it predicts that this modulation appears, relative to stimulus onset, first in the hippocampus followed by the SN. Third, if relevant for declarative memory, SN activity during novel stimuli should be predictive of the success or failure of memory formation as assessed by later behavior. Here, we test these three predictions directly in humans by recording the activity of individual SN neurons and relating their activity to behaviorally assessed memory strength.

Our subjects performed a recognition memory task for which we and others have described novelty-signaling neurons in the human hippocampus [25]. The extent to which these

memory-selective neurons are modulated by ongoing theta oscillations is predictive of the success or failure of memory formation [26]. Dopamine is thought to be essential for the success of memory formation in this task, raising the question whether or not the activity of SN neurons is additionally coordinated by ongoing theta oscillations. Theta-frequency and other low-frequency oscillations are critical in coordinating information flow between cortical and subcortical areas [27–29], including the SN/VTA, the hippocampus, and cortex. However, it remains unknown whether coordination of neural activity between SN neurons and cortex also plays a role in declarative memory formation. Here, we simultaneously recorded the activity of SN neurons together with cortical field potentials over the frontal lobe to assess whether the activity of SN neurons is coordinated with cortical activity and whether such coordination is predictive of the success of memory formation.

Results

Task and Behavior

23 subjects (28 sessions; see Table S1) undergoing implantation of a deep-brain stimulation (DBS) device in the subthalamic nucleus (STN) for the treatment of either Parkinson's disease (PD) or essential tremor performed a continuous recognition memory task. Two recording sessions were excluded because subjects performed at chance level, and three sessions were excluded because recordings were made outside of the SN (see Figures 1D and 1E). Thus, 23 sessions remained for analysis.

Subjects were asked to view a sequence of images and to identify each image as novel or familiar (Figure 1B). Subjects pressed either the "new" or "old" button to provide their answers (button identity was reversed in the middle of the experiment). Each image was presented up to three times. The first presentation is referred to as "novel" and the remaining two presentations as "familiar". Subjects performed well, with an average recognition accuracy of 82% ($\pm$8%, $\pm$SD; Figure 1C). Also, subjects continued learning as demonstrated by a significant performance increase during the second familiar presentation (87% $\pm$ 13%) compared to the first one (74% $\pm$ 12%, t [22] = 5.62, p = 0.0005, permutation paired t test). Only correct trials were used for analysis unless stated otherwise. The median time between onset of the question screen and button press was 0.69 $\pm$ 0.99 s, with no significant difference in reaction time between novel (1.12 $\pm$ 1.06 s) and familiar responses (1.05 $\pm$ 0.90 s, t [22] = 1.17, p = 0.26, permutation paired t test). The images we used each belonged to one of three different visual categories (animals, landscapes, and fruits). There were no significant differences in reaction time as a function of visual category (one-way permutation ANOVA: F [2,44] = 2, p = 0.13). Together, these behavioral data show that patients performed the task accurately. Pre-operative neuropsychological evaluation testing was consistent with this observation (see Table S1).

Electrophysiology

We identified 66 well-isolated putative single neurons recorded from the SN. Figures 1D and 1E show the locations of all recording sites in Talairach space as determined from stereotactic coordinates (also see STAR Methods and Figures S2E and S2F). Neurons were well isolated as assessed quantitatively using spike sorting quality metrics (Figure S1).

Throughout the manuscript, we use the terms neuron, unit, and cell interchangeably to refer to a putative single neuron. From each microelectrode, we also recorded field potentials using the low-impedance electrode contact located 3 mm above the microelectrode tip (Figure S2A). In addition, we recorded cortical surface (electro-corticography [ECoG]) signals using a subdural strip electrode placed along the dorsal fronto-parietal brain surface, extending anterior and posterior to the central sulcus (Figures S2B–S2D). We localized the position of the ECoG electrodes and their related cortical areas using a combination of intraoperative imaging and median nerve stimulation (see STAR Methods and Figures S2C and S2D). The median location of all ECoG recordings is shown in Figure 1F.

SN Neurons Respond to Visual Stimuli

We first tested whether neurons changed their firing rate in response to image onset when considering all trials together, regardless of novelty/familiarity (see STAR Methods). We found that 14/66 (21.2%, p = 0.002, compared to null distribution; Figure 2A) of neurons changed their firing rate in response to image onset (comparing spikes in a window 0–1.5 s following stimulus onset with a window –0.5–0 s preceding stimulus onset). Of these "image responsive" neurons, five increased their firing rate relative to baseline (example neuron shown in Figure 2C) and 9 decreased their firing rate (example neuron shown in Figure 2D). The neurons that increased their firing rate responded significantly faster than those that decreased their firing rate (224.8 ± 138.5 ms versus 426 ± 141.9 ms, t [12] = 2.58, p = 0.03, permuted t test; see Figure 2B).

In many human brain areas, neurons differentiate between visual categories [30]. We therefore next asked whether the response of SN neurons differentiated between the three different visual categories (animals, landscapes, and fruits) of the images. We did not find evidence for SN category neurons: a one-way permutation ANOVA did not reveal a significant number of neurons tuned to visual category (N = 6, 9.1%, p = 0.16; Figure 2A). In contrast to the medial temporal lobe (MTL) [30], we did not find a visual category signal in the SN.

SN Neurons Differentiate between Novel and Familiar Stimuli

We next tested whether SN neurons signaled that a stimulus is novel (shown the first time) or familiar (shown the second or third time). Here, we refer to such neurons as memory-selective (MS) neurons [25]. We tested whether the response of SN neurons exhibited this pattern by comparing the responses of neurons following stimulus onset between novel and familiar trials. We first focused on the subgroup that had a larger firing rate for novel relative to familiar stimuli (see STAR Methods). We identified 11 such neurons (Figures 3A–3C; 16.6%, p = 0.002, compared to null distribution; see also Figure S3A). We refer to this subset of MS neurons as "novelty" neurons. This difference in response between novel and familiar stimuli was already apparent when the image was seen the second time (Figure 3D, middle). The response remained but did not strengthen further when comparing the second and third presentation of the same image (t [10] = 1.36, p = 0.21, permuted paired t test; see Figure 3D, right). Additionally, the difference in response between novel and familiar stimuli did not depend on the delay between two consecutive presentations of the same image (F [3,30] = 0.22, p = 0.88, one-way permutation ANOVA; see Figure 3E).

We next tested whether other SN neurons increase their firing rate in response to familiar images. We found that 6 neurons (9%, p = 0.01, compared to null distribution; see also Figure S3B) showed a significant increase for familiar compared to novel images. Similar to novelty neurons, the response of such "familiarity" neurons did not change further between the second and third presentation of the same image (t [5] = 0.7, p = 0.06; Figure 3D) and was not modulated by the length of the delay between consecutive presentations of the same image (F [3,15] = 2.12, p = 0.14; Figure 3E). Together, these data demonstrated that the firing rates of a substantial proportion of SN neurons (16.6% and 9.0%; Figure 3A) were modulated by the novelty or familiarity of images in a declarative memory task. Importantly, this change in response was visible after a single learning trial (Figure 3D) for both novelty and familiarity neurons.

We refer to the 17 novelty and familiarity neurons together as MS neurons (Figure 3A). 4 MS neurons also qualified as image-responsive neurons (i.e., they showed a change in firing rate for all trials considered together; see Figure 2). The reason for this small overlap is the absence of a response to the non-preferred stimulus category. To show this, we compared the firing rate of only the novel or familiar trials (depending on what type of trial the neuron was sensitive to) with the baseline firing rate. This revealed that MS cells had a significantly higher firing rate during image presentation (0–1.5 s, 7.23 ± 17.9 Hz) compared to baseline (−0.5–0 s, 6.2 ± 20.9 Hz, t [16] = 1.38, p = 0.042, permuted paired t test), but only for their preferred type of trial (novel or familiar; note that this is not by selection because the baseline firing rate is not considered when selecting MS neurons).

We performed additional control analyses to verify that this memory signal was not due to other factors, such as electrode drift or slow firing rate changes. First, we verified that no similar difference existed during the baseline period: neither noveltynor familiarity-type MS neurons showed such a difference (Figure 3D, left; not significantly different versus 0 for novelty neurons [t [10] = 0.07, p = 0.94] and familiarity neurons [t [5] = 0.58; p = 0.54]). We also tested how many MS neurons would be selected if we used the baseline period (−0.5–0 s) rather than the after-stimulus onset period for selection. This analysis revealed only 1 (1.5%) out of 66 units with a significant difference between novel and familiar images. Finally, we used a mixed-effect regression model to identify factors that explain variance in the firing rate of MS neurons. As predictors, we used image familiarity and trial number (plus neuron cluster ID was used as a random effect). This analysis revealed that the image familiarity regressor was significant even after accounting for effects of trial number and was much stronger than the trial number regressor for both MS neuron types (novelty neurons: t [864] = 8.95, p < 1e–30 for new/old regressor versus t [864] = 1.67; p = 0.09 for trial number regressor; familiarity neurons: t [501] = 7.24, p < 1e–12 for new/old regressor versus t [501] = 3.67, p = 0.0002 for trial number regressor). Lastly, note that we randomly intermixed novel and familiar stimuli throughout the experiment. Together, these control analyses verify that the difference in responses cannot be attributed to electrode drifts.

SN MS Neurons Predict Behavior

We next investigated whether the response of MS neurons (tested separately for novelty- and familiarity-preferring neurons) was related to memory by assessing whether their response

co-varied with the behavior of the subject. Specifically, we compared the neural responses to familiar stimuli (those which have been shown at least once before) that the patients correctly remembered (response "old") to those they mistakenly forgot (response "new"). Behaviorally, patients showed good performance: they remembered (true positive rate) 74% of images during the first repetition ("familiar 1") and 87% after the second repetition ("familiar 2"). We found that the response of novelty cells was significantly attenuated during trials in which familiar images were mistakenly rated as novel compared to when they were correctly rated as familiar, with a firing rate difference of 0.36 ± 0.36 Hz for incorrect and of 0.60 ± 0.24 Hz for correct trials (see Figure 3F; t [11] = 2.72, p = 0.02, permuted paired t test; the metric used was the difference in firing rate between when an image was novel and familiar normalized by the baseline firing rate). For this comparison, we excluded trials for which the initial novel presentation was incorrect (a false positive), so the difference observed could only be attributed to forgotten images (false negatives). However, although smaller, the response to forgotten familiar stimuli was still significantly different from zero (Figure 3F; t [11#x0005D; = 3.98, p = 0.002, permuted t test). Together, this analysis shows that the response of novelty neurons was indicative of whether a familiar stimulus would be remembered or forgotten. For neurons that increase their firing rate (n = 6) to familiar images, this behavior-neuronal activity correlation was quantitatively similar, but not significant (Figure 3F; t [5] = 2.31, p = 0.056).

Latency of Response

How quickly after stimulus onset did the response of MS SN neurons differentiate between novel and familiar images? To answer this question, we next estimated the first point in time at which responses differed between novel and familiar images. We compared the cumulative sum of the spike trains, a method that provides an estimate of the differential latency of a neuron with high precision [31]. We found that the average differential latency was 527 ms after image onset (Figure 3G). We compared this latency with the latency of MS neurons (n = 122) recoded in the MTL during a similar new/old recognition task in another patient population [32, 33]. MS neurons in the MTL had an average differential latency of 311 ms, which was significantly faster compared to the SN (p = 0.013, estimated based on an empirically estimated null distribution for which area labels were randomly re-assigned). This result was also true when considering MS neurons that increased their firing rate to novelty and familiar stimuli separately (p = 0.002 and p = 0.002, neurons, respectively, compared to n = 64 novelty and n = 58 familiarity neurons in MTL). This order of responses is compatible with the Lisman and Grace model of the interaction between the hippocampus and the VTA/SN [9].

Cell Type Analysis

The SN contains two principle types of neurons: inhibitory GABAergic neurons and dopaminergic neurons that project to remote targets, including the striatum, amygdala, and hippocampus [4, 34–36]. Using extracellular recordings, different cell types can often be distinguished based on a combination of the width of the extracellular spike waveform and mean firing rate [37]. In particular, in the SN, it is known that dopaminergic neurons have wider waveforms and lower firing rates compared to GABAergic neurons [38, 39], which results in a bimodal distribution of the waveform width across all neurons. We found that,

across all recorded neurons (N = 66), the distribution of spike widths was bimodal (Hartigan's dip statistic: 0.0717, p = 0.006 [40]; see Figures 3H and 3I). We thus next investigated whether MS neurons were preferentially of a certain cell type. We found that MS neurons were on average characterized by longer waveforms compared to non-MS neurons (1.15 ± 0.23 ms versus 0.96 ± 0.32 ms; waveform length was measured as the time that elapsed between the two positive peaks [14] of the waveform; t [65] = 2.65, p = 0.012, permutation t test; Figures 3H and 3I). Additionally, MS neurons satisfied the criteria for DA neurons established by previous work: 15/17 MS neurons had waveforms longer than 0.8 ms and firing rates lower than 15 Hz [14, 41]. We also found that the recording sites where MS neurons were identified were predominantly in the dorsal parts of the SN (Figures 1D and 1E). These results are consistent with the location of the pars compacta, in which the majority of dopaminergic neurons are located [42, 43]. Together, these analyses support the view that the MS neurons we identified were putatively dopaminergic.

SN-Cortex Interactions

Was the activity of SN neurons related to field potential activity recorded from the basal ganglia and/or the cortical surface? We quantified spike-field interactions using spike field coherence (SFC) as a metric to answer this question. First, the SFC between SN neurons and the field potentials recorded in the basal ganglia (STN) was significantly above chance in the theta-frequency band (Figure 4A, left panel; significant at p < 0.05 in 2-5 Hz across all N = 56 neurons with enough spikes). Note that here the field potential was most likely recorded from the STN and not the SN due to the location of the recording contact 3 mm above the microelectrode tip (see STAR Methods and Figure S2A). Second, SN neuron activity was also coordinated with cortical field potentials: SN neurons had a preference to fire more during certain phases of the theta and alpha frequency band of ECoG signals recorded from the cortical surface (SFC was significantly different in the 6–12 Hz frequency band, N = 61, p<0.05; Figure 4A, right panel; see legend for statistics; see also Figure S4 for all electrodes). This was true only for one pair of ECoG contacts located anterior to the central sulcus (labeled as +2; other contacts were not significant; see Figure S4). The +2 ECoG contacts were located on the superior frontal gyrus in Brodmann area 6 (premotor cortex). This finding indicates that SN neuronal activity is functionally connected to this region of the frontal lobe (see Discussion). We next tested whether this functional connection was behaviorally relevant by comparing its strength between novel trials that were later remembered with novel trials that were later forgotten.

Based on previous research and model predictions [26], we hypothesized that the extent of spike-field coherence during encoding of novel images predicts whether subjects would successfully encode a new memory or not. To test this hypothesis, we compared the SFC during viewing of novel images between trials that were later remembered correctly versus trials that were later forgotten (i.e., identified as novel). This difference-due-to memory comparison showed that images that were later remembered were accompanied by higher SFC in the theta frequency range for ECoGs measured anterior to the central sulcus during encoding (N = 58 neurons, 3-9 Hz, p < 0.05; Figure 4B, right panel; see legend for statistics). Note that this calculation only includes trials during which the image was seen for the first time (novel) and which the subject correctly labeled as "new." Therefore, the

response was always the same ("new"), excluding the possibility that this difference was due to differences in motor planning. Similar to the SFC considering all trials, this difference was only significant for field potentials recorded from the anterior +2 contact located on premotor cortex (central sulcus +2; Figure 4B; Figures 4C and 4D show an example neuron's SFC and spike triggered average). We did not observe a similar relationship with field potential recordings from the basal ganglia (STN; Figure 4B, left panel; all p > 0.05). As a control, we also compared ECoG power between the two conditions but found no significant differences (Figure 4E; all p > 0.05). Together, this shows that the extent of long-range SFC between SN neuronal activity and frontal cortical field potential activity recorded from premotor cortex was predictive of successful memory formation.

How could this long-distance spike/field coordination be achieved? To answer this question, we next performed a phase-coherence analysis between the field potential recordings in basal ganglia (STN) and ECoG recordings from cortex obtained while patients viewed the novel images (0–1.5 s relative to stimulus onset; see STAR Methods). This analysis showed that successful encoding of new memories was associated with significantly higher phase coherence in the theta frequency range (5–10 Hz; Figure 4F; p < 0.05; see legend for statistics). Similar to the SFC finding, this effect was observable only on the central sulcus +2 electrode (Figure 4G). The power of the ECoG signals recorded from the central sulcus +2 electrode exhibited a prominent beta-band power decrease starting about 500 ms after stimulus onset, which was most likely related to movement preparation (Figure 4H). This beta decrease was preceded by an increase in theta frequency power (Figure 4H), which started shortly following stimulus onset. This pattern shows that processing an image increases the power of theta oscillations in frontal cortex, which provides a potential mechanism by which SN neurons could modulate the extent of coordination between their activity and frontal cortical theta. Here, we show that the extent of such phase locking is predictive of memory encoding success, which suggests that theta frequency range oscillations coordinate information transfer between areas during memory encoding.

Discussion

We found that the activity of individual neurons in the human substantia nigra differentiates between novel and familiar images in a hippocampal-dependent declarative memory task. Additionally, we found that the degree of coordination of the activity of SN neurons with frontal theta frequency oscillations was predictive of successful memory formation. Although previous work shows that human SN neurons respond to reward prediction errors [14] and infrequent sounds in an odd-ball paradigm [16], our data are, to our knowledge, the first study describing SN neuronal activity during declarative memory formation in humans.

The electrophysiological properties of the memory selective cells we describe indicate that these cells are most likely dopaminergic. This conclusion rests on two pieces of data: the width of their waveforms and anatomical location. Dopaminergic neurons have considerably wider extracellular waveforms compared to the GABAergic neurons also located in SN [38, 39, 44]. Also, although dopaminergic neurons exist throughout the SN, the majority are located in the pars compacta subregion of the SN [42, 43]. Most dopaminergic neurons should therefore be located in the dorsal-medial part of the SN, which is the area where we

found the majority of MS neurons. Together, these criteria have been demonstrated to reliably separate dopaminergic and GABAergic neurons in the SN based on electrophysiological features alone [38, 39, 44–46]. A definitive confirmation of this assertion will require either histological analysis [47] or genetic targeting [38]. Here, we refer to these neurons as putatively dopaminergic to indicate that this conclusion rests on extracellular recordings alone.

A second consideration is the effect of ongoing neurodegeneration on our results. The majority of the subjects in the study had PD and therefore suffered from a substantial loss of dopaminergic cells in the SN. However, our recordings accessed an anatomical area where a sufficient population of dopaminergic neurons is still functional even in PD. Dopaminergic loss in PD progresses unevenly [48, 49], targeting some areas more severely than others. Post mortem tissue analyses in PD patients typically show high loss of dopaminergic neurons in the caudal part of the SN, with approximately 90% of cells lost. In contrast, cell loss in more dorsal areas is more moderate (50% or less) to a degree comparable with what can be observed in normal aging [49]. Indeed, several studies have succeeded in recording from putative dopaminergic neurons in patients with PD undergoing STN DBS surgery [14, 41]. With the surgical target in the STN, it is reasonable to expect SN recordings to be located predominantly in the dorsal area of the SN. This assumption was confirmed by the analysis of our electrode positions, which showed most recordings located in the dorsal part of the SN, where disease impact is expected to be relatively minor [49]. It remains unknown, however, whether PD could have influenced the waveforms of the remaining DA neurons that we recorded. Although we did not detect a correlation of disease severity with waveform duration (see STAR Methods), this issue remains an open question. Finally, the patients enrolled in our study were at considerably earlier PD stages than those included in post mortem analysis [48, 49], therefore preserving a higher density of dopaminergic cells in the dorsal areas of the SN.

It has been proposed that the role of dopaminergic modulation of hippocampal memory processes is to enhance synaptic plasticity for important events, such as those that are rewarding, aligned with a subject's goals, or that attract attention [9, 23]. The proposed pathway for this signal to reach the SN/VTA is through afferents from the nucleus accumbens (NA) and pedunculopontine tegmental nucleus (PPTg), which are both structures involved in mediating motivational and attentional processes [50, 51]. Both NA and PPTg in turn receive inputs from the prefrontal cortex (PFC) and the hippocampus, enabling them to integrate signals about current goals and stimulus novelty [23, 50, 51]. It has been hypothesized that hippocampal novelty signals cause dopamine release within the hippocampus through this multisynaptic pathway [9, 23]. Here, we identified putative dopaminergic neurons within the SN that are compatible with this hypothesis because they respond with an increase in firing rate to novel stimuli. Interestingly, in addition to novelty neurons, we also identified a smaller group of putative dopaminergic neurons that responded with an increase in firing rate to familiar stimuli. The response characteristics of this group of neurons were otherwise similar to novelty neurons (Figures 3D, 3E, and 3H), with the exception that they were not significantly indicative of whether a familiar stimulus would be remembered or forgotten (but note that this is most likely due a lack of statistical power). Although those neurons are not directly predicted by the theoretical model of Lisman and

Grace, it is likely that they also play a role in learning. For example, different concentrations of DA can lead to either synaptic depression or potentiation [52] and levels of DA can control the long-term potentiation (LTP)/long-term depression (LTD) threshold [53]. This suggests that neurons that increase levels of DA for familiar stimuli might participate in maintaining this homeostasis. Additionally, different types of dopamine receptors have different sensitivities and activation thresholds and mediate different aspects of plasticity, including encoding versus consolidation of memories [54, 55]. Together, this literature combined with our finding supports the hypothesis that familiarity neurons have a role in the plasticity mechanisms that serve to strengthen already encoded memories. Future work is needed to directly test this hypothesis.

The latency of the SN responses was also compatible with the Lisman and Grace model, namely that SN MS responses emerged significantly later compared to those observed in the MTL [33]. Here, we found that SN responses were first visible 527 ms after stimulus onset, a time which was larger than the 311 ms interval observed in the MTL [32]. A caveat of this comparison is that it was derived from two different patient populations (PD and epilepsy, respectively). Together, our results support the idea that the information about stimulus novelty observed in the SN originates in the MTL. Importantly, the extent of the modulation of SN cells was indicative of whether a subject would correctly recognize a familiar stimulus. This result indicates that the response of SN cells was behaviorally relevant for the declarative memory task that our subjects performed. This finding is also in line with human studies showing that SN fMRI-blood-oxygen-level-dependent (BOLD) activity predicts successful memory formation [5, 6]. However, it remains unknown what the relationship is between the activity of different cell types in the SN and the BOLD signal (but see [56]). In contrast, here we identified specific SN cell types electrophysio-logically and showed that it is the phasic activity of putative DA neurons shortly after stimulus onset that is predictive of memory formation.

We observed that the activity of SN neurons was systematically related to the phase of ongoing theta oscillations in the frontal cortex (measured over the premotor cortex). This coordination was behaviorally relevant because the extent of phase locking was predictive of memory formation success. Oscillations in the theta frequency range are thought to coordinate information flow between the MTL, basal ganglia, and frontal cortex [27–29]. Here, we now show that, in humans, SN neuronal firing is related to cortical theta frequency oscillations and that such coordination is behaviorally relevant for memory formation. The importance of theta synchrony between the basal ganglia and frontal cortex has been established by previous recordings of human patients performing cognitive tasks [57, 58]. Interestingly, slow 4 Hz stimulation of the STN improves performance in cognitive tasks [58]. A key unknown question is whether the theta oscillations we quantified are related to or synchronized with hippocampal theta [27–29].

Antidromic stimulation of the STN evokes short latency responses in premotor cortex, which is compatible with a "hyperdirect" pathway in humans [59]. There are thus at least three pathways by which information from the MTL could reach the SN: (1) via the NA and PPTg; (2) via the hyperdirect route; and (3) through the striatum, which is interconnected with most of the frontal cortex [60]. This rich innervation most likely gives rise to the

functional dependency of SN and frontal cortex as observed using BOLD-fMRI [61, 62]. Also, BOLD activity in frontal cortex predicts successful encoding of new memories [63], a signal which is thought to be a reflection of the role of frontal cortex (including premotor areas) in facilitating the encoding of goal-relevant information and in organizing multiple pieces of information into an individual memory [63]. Here, we now show a possible mechanism by which such information could influence the strength of memory encoding by modulating dopaminergic SN activity. A key future experiment will be to determine whether SN neuronal activity is also coordinated with hippocampal theta oscillations and how these theta oscillations relate to the frontal cortical theta oscillations measured here.

Star⋆Methods

Key Resources Table

REAGENT or RESOURCE	SOURCE	IDENTIFIER
Software and Algorithms		
MATLAB R2016a	MathWorks	SCR 001622
OSort	http://rutishauserlab.org/osort/	SCR 015869
Psychophysics toolbox PTB3	http://psychtoolbox.org/	SCR 002881
EEGLab	SCCN	SCR_007292
Other		
Alpha Omega MicroGuide System	Alpha Omega (https://www.alphaomega-eng.com/)	AlphaOmega Microguide
Alpha Omega Hybrid Microelectrodes	Alpha Omega (https://www.alphaomega-eng.com/)	Cat# STR-000021
Ad-Tech 8-contact ECog strips	Ad-Tech (https://adtechmedical.com/subdural-electrodes)	Cat#IS08RSP10X-0T1
Cedrus Response Box	Cedrus (https://cedrus.com/)	Cat#RB-844

Contact For Reagent and Resource Sharing

Further information and requests for resources should be directed to the Lead Contact, Ueli Rutishauser.

Experimental Model and Subject Details

23 patients with Parkinson's Disease (PD) and two with Essential Tremor undergoing implantation of a DBS electrode in the subthalamic nucleus (STN) volunteered for the study and gave written informed consent (see Table S1). Surgical indications for DBS followed established guidelines [64]. This study was approved by the Institutional Review Board of Cedars-Sinai Medical Center. All patients undergoing surgery underwent pre-operative neuropsychological testing that confirmed the absence of severe cognitive abnormalities that would have precluded DBS (see Table S1 for neuropsychological scores). For patients

requiring bilateral implantation a second surgery was performed 1-2 weeks after the first surgery. To test whether the severity of PD of a patient could have affected our recordings we correlated electrophysiological measures (waveform properties, mean firing rate, proportion of novelty neurons identified) with the Unified Parkinson Disease Rating Scale (UPDRS) score (measured when DBS was Off). However, we did not find any significant correlations. Here we report some of the correlations: UPDRS versus mean waveform length r = −0.25 p = 0.34; UPDRS versus mean firing rate r = −0.21 p = 0.43; UPDRS versus number of novelty neurons r = −0.45 p = 0.11. This shows that in this surgical patient sample, PD severity did not correlate with features of our electrophysiological recordings.

Method Details

Task—Subjects performed a continuous recognition memory task, during which they classified a series of images as novel or familiar (Figure 1B). Images were shown on an LCD screen positioned 60 cm in front of the subject's face, resulting in an image size of 18 degrees of visual angle. Each trial started with fixation cross shown for 0.5-1.0 s (randomized). Afterward, an image was shown for 1.5 s. Each image belonged to one of three visual categories (animals, landscapes, fruits; one third each). After image offset, a fixation cross was shown for 0.5 s, followed by the question screen (Figure 1B). This screen stayed on the screen until patients made a response (no timeout). Participants responded by pressing either the green or red button on a response pad (RB-844, Cedrus Inc) using the hand contralateral to the side of recording. Which color corresponded to 'new' and which to 'old' was shown at the top of the question screen. We used this approach to switch the location of the 'new' and 'old' buttons in the middle of the experiment as a control. This switch did not significantly impact behavioral performance (accuracy just before switch was 86% ± 34%, compared to 82% ± 28% after the switch (t [24] = 0.37; p = 0.97). Trials with new and old images were intermixed. Each session of the experiment consisted of 108 trials, during which 54 unique images were shown up to three times. The task was implemented in MATLAB using the Psychophysics Toolbox [65].

Target planning—DBS electrodes were inserted using a well-established technique [66]. Briefly, prior to surgery patients underwent a 3T T1 weighted and T2 weighted high resolution (2mm slice thickness) MRI of the brain. The MRI provided high resolution visualization of the STN and other deep brain nuclei to aid in surgical planning. On the morning of surgery, patients had a stereotactic frame (CRW, Integra) secured to their head, followed by a CT scan (1.25 mm contiguous slices from vertex to foramen magnum, 0-degree gantry angle) with a fiducial localizer attached to the frame during scanning. The CT scan and the previously acquired MRI scan were then co-registered (Framelink, Stealth Station Medtronic, Inc; see Figure S2E). Next, we defined the location of the anterior and posterior commissures, with the resultant mid-point of the AC-PC (commissural) line defining the center (X = 0, Y = 0, Z = 0) of the coordinate system used. The STN target was then selected using standard atlas based methods (x = +/−12.0, y = −4.0, z = −4.0) and refined based on patient specific anatomy. An entry point was selected, typically anterior to the coronal suture and approximately 3 cm lateral to midline, roughly 60 degrees anterior and 15 degrees lateral to the vertex of the frame. The entry and target points (and associated trajectory) were then further adjusted based on each patient's anatomy. The goal of planning

was to define a trajectory that minimized traversing of brain sulci, avoided the lateral ventricle of the brain, and traversed along the long axis of the STN. The SN is typically situated 2-3 mm below the STN, but can vary from being directly adjacent to up to 4-5 mm deep.

Surgery—In the operating room, the patient was sedated and long-lasting lidocaine was used to anesthetize the skin. The planned entry site was shaved, prepared, and draped in sterile fashion. The target coordinates were manually set on the CRW arc and placed onto the frame. The microdrive (Alpha Omega, Nazareth, Il.) was positioned on the frame and once the skin was opened, the exact angle and location of the entry point was marked on the skull using a guide cannula. A drill was then used to create a 10mm bur hole directly over this site. Once the hole was drilled a plastic outer ring was placed around the hole for later locking of the electrode. The dura was then opened widely and the cortex exposed. An 8-contact strip (Ad-Tech, IS08RSP10X-0T1) electrode was then passed into the subdural space in a posterior and slightly lateral trajectory until all electrodes made contact with the brain surface. The strip electrode invariably extended posterior to the central sulcus, with electrodes covering the pre-and post-central sulci as well as the pre-motor cortex (see Figures 1F, S2C, and S2D). The microdrive was then aligned directly over the bur hole and one or two guide cannulas (15mm length, Alpha Omega STR-000021) were inserted into the brain, one aimed directly along the planned target, and a second one 2mm either lateral, medial, anterior, or posterior to the target trajectory as indicated by the likely best secondary trajectory to the STN. Once both guide cannulas were placed the burr hole was covered with a dural sealant (DuraSeal, Integra) to prevent egress of CSF and minimize brain shift. Microelectrodes were then inserted and recordings were started 25mm above the planned target.

Electrophysiology—We used a microelectrode (Alpha Omega, STR-000080-0024950; see Figure S2A) that contains both a tungsten microeletrode (~0.5 MΩ impedance) and a lower impedance (3.2 kΩ) macro contact for field potential recordings that is located 3 mm above the microelectrode tip. For signal acquisition, we used either an Alpha Omega MicroGuide or Neuroomega system. ECoG and field potentials signals were recorded using a 1-1000 Hz bandpass filter. Microelectrode recordings were performed using a 250–6000 Hz bandpass filter. As reference for the ECoG recordings we used one of the contacts located on the cortical strip. As reference for the microelectrode we used the electrode cannula. Because of technical problems we did not record the basal ganglia field potentials signal in two sessions. Also, a further session did not have usable ECoG recordings.

Localization of electrodes—Once the electrodes were placed the patient was awakened from sedation. Recordings were not started until the patient was alert and responsive. Continuous ECoG was recorded while the microelectrodes were advanced toward the STN, typically in increments of 1 mm until the STN was encountered and 0.3-0.5mm steps once the STN was encountered. The STN was identified based on the characteristic neuronal discharge pattern of large, irregular, high amplitude and high frequency discharges with a thickened baseline [67]. The STN was typically recorded for a length of 2.5-5 mm, after which a quiet zone was encountered, with re-emergence of high amplitude, high frequency

neurons at 0-3 mm below the STN, identifying the SN [67]. Microelectrode recording locations were identified and documented based on the pre-operative planning (Figure S2E). In addition, in a subset of cases where localization was uncertain, we used electrical microstimulation (10 mA, 500 ms duration, 200 Hz frequency) to further confirm positioning (Figure S2F). This stimulation procedure allowed us to reliably differentiate STN from SN because weak electrical stimulation transiently inhibits activity of SN but not STN neurons (see Figure S2F for an example) for several hundred ms after the offset of stimulation [67]. Talairach coordinates of the final recording position were determined using the StealthStation software by appropriately adjusting the original plan with modifications made during surgery. Talairach coordinates for one session were unrecoverable for technical reasons.

The ECoG strip was localized based on two methods: first, we used median nerve stimulation of the contralateral hand (20–30 mA, Cadwell Elite system; see Figure S2B for an example) in order to locate the central sulcus based on the location of the evoked potential polarity reversal [68]. Second, in a subset of cases (6 sessions), we acquired intra-operative X-ray images (lateral and AP) while the ECoG strip was in place. We then utilized the LOC software package [22] to merge this image with the FreeSurfer reconstructed cortical surface [69] (see Figures S2C and S2D for an example) as determined from the pre-operative MRI scans [70]. Comparing the results of this procedure with the result of median nerve stimulation revealed that median nerve stimulation alone was highly accurate. For this reason, we subsequently relied exclusively on median nerve stimulation to localize the ECoG strip. For analysis purposes, we assigned to each pair of channels a number of –1, 0, +1, +2 or +3, which indicates the location of an ECoG contact relative to the central sulcus (see Figure 1F). All ECoG analysis was based on bipolar re-referenced channels to remove common effects of activity present on the reference (see Figure 1F for pairs used). Thus, the numbers –1 through +3 indicate pairs of channels that were subtracted from each other before analysis.

Quantification and Statistical Analysis

Spike sorting and quality metrics of single units—The raw signal was filtered with a zero-phase lag filter in the 300 to 3,000Hz band, and spikes were detected and sorted using a semi-automated template-matching algorithm [71]. We computed the following spike sorting quality metrics for all identified putative single units to assess their quality (Figure S1): (i) the percentage of interspike intervals (ISIs) below 3 ms was $0.22\% \pm 0.43\%$; (ii) the ratio between the s.d. of the noise and the peak amplitude of the mean waveform of each cluster was 2.92 ± 1.07 (peak SNR); (iii) the pair-wise projection distance in clustering space between all neurons isolated on the same wire was 12.31 ± 6.67 (projection test; in units of s.d. of the signal) [72]; (iv) the modified coefficient of variation of variability in the ISI (CV2) was 0.9 ± 0.08; and (v) the mean isolation distance [73] was 102.2. We calculated the isolation distance in a ten-dimensional feature space (energy, peak amplitude, total area under the waveform and the first five principal components of the energy-normalizes waveforms [73]).

Statistics—Unless otherwise noted, all statistical comparisons were conducted using non-parametric permutation tests. The null distribution for each statistic was estimated by scrambling the order of trial labels randomly (repeated 2000 times). This procedure was used as implemented in the EEGLAB toolbox [74]. For comparisons between two groups, we used t-statistics (referred to as permuted t test). For comparisons with more than two conditions, we used F-statistics. In either case, the t and F statistics were estimated using the empirically estimated null distribution instead of their parametric versions. As a consequence, note that the reported p values may differ from those expected from the t- and F-distribution.

Single neuron analysis—The mean activity of each cell was computed in bins of 400 ms width that were advanced in steps of 1ms. To determine whether the activity of a cell differentiated between two conditions (three for visual categories), we statistically compared the mean activity in each group in every such bin located within the time period of 0-1.5 s relative to stimulus onset (see above for description of the permuted t-and F statistics used).

We used a cluster-based approach to correct for multiple comparisons [75]. For this purpose, a cluster is defined as a group of adjacent tests that are all significant at p < 0.05. For all such identified clusters, we tested whether the summed value of the test statistic across all values that are part of the cluster was larger than the 95th percentile of the same value estimated from the null distribution (based on scrambled labels). Clusters that did not exceed this value were removed from the list of significant time points. When at least one cluster passed this correction for multiple comparisons, that neuron was considered as significant. To determine whether the number of selected neurons for a given comparison was larger than that expected by chance we compared the number of actually selected neurons to that selected when repeating the same procedure after randomly scrambling the trial labels (repeated 500 times). This provided a null distribution for assessing the probability of observing a given number of neurons by chance. To test if the firing rate of a neuron changed in response to the onset of a stimulus we compared mean firing rates between the period of time before image onset (–0.5-0 s relative to image onset) with each bin of the PSTH after image onset (0-1.5 s, corrected for multiple comparisons as described above). To determine whether the number of selected neurons for this selection was larger than that observed by chance we compared the number of actually selected neurons to that selected when repeating the same procedure on data with scrambled labels (baseline versus after image onset period, repeated 500 times).

To select MS neurons, we used the following procedure. We first compared whether the firing rate, after stimulus onset (0-1.5 s), differed between novel and familiar stimuli (as described above using a two-tailed permutated t test with cluster correction [75]). For every neuron that satisfied this criterion, we then labeled the neuron as a novelty- or familiarity-type according to which trial type had a higher firing rate relative to the other condition (novel > familiar and familiar > novel, respectively).

To summarize the response of MS neurons, we used as a metric the ratio between the mean response to novel minus the mean response to familiar stimuli (counting only spikes that occurred during the period of time during which the comparison used to select the neuron

was significant), divided by the baseline firing rate of the neuron over the entire task (Figures 3D–3F). We multiplied this metric by −1 for neurons that responded more strongly to familiar than to novel images.

Differential latency analysis—To compute the point in time at which a neuron's response first differentiated between two conditions we used a differential latency approach. We first binned the spike trains of each trial into 1-ms bins and computed the cumulative sum [31]. Second, we averaged the cumulative sums of all trials of a neuron that belong to the same condition. We then compared the difference between the two cumulative sums with zero using a permutation t test to find the points of time at which they were significantly different. The latency is defined as the first significant bin which passes the cluster correction for multiple comparisons [75].

Field potential analysis—The SFC is the ratio of the spectrum of the spike triggered average (STA) normalized by the averaged spectra of the traces used for constructing the STA [26, 76]. The STA was computed by averaging short segments of 1 s length (±500 ms centered on each spike) of the field potential. Field potentials were high-pass filtered at 1Hz before the spike-triggered snippets were extracted. All spikes from 0-2.5 s following stimulus onset were used. The spectrum was calculated using multitaper analysis using 5 tapers and a time-bandwidth product of 3 (Chronux toolbox [77]). For Figure 4A, the null distribution was estimated by adding a random time (at least 1s, at most the remaining length of the experiment -1s, uniformly distributed; spike times were wrapped around to assure that none were located outside of the experiment) to the entire spike train and repeating this procedure 500 times. Using this null distribution, we then tested whether the observed SFC value at a given frequency was larger than expected by chance using a permutation t test. For each SFC comparison we used a cluster-based approach to correct for multiple comparisons [75]. To compare the SFC between two experimental conditions, we equalized the number of spikes used for each condition by taking a random subset of spikes from the condition with more spikes. The reason for this is that the SFC is biased by the number of spikes used [78]. For visualization only, we in addition z-scored the SFC with respect to the mean and standard deviation across all conditions and frequencies of a cell before averaging across cells. When comparing forgotten and remembered familiar trials, only the first repetition ("familiar 1") was used. The computation of SFC for basal ganglia and cortex include different numbers of cells (56 versus 61, respectively) because we did not record basal ganglia field potentials signal in two sessions due to technical problems. Also, a further session did not have usable ECoG recordings due to problems inserting the electrode strip. For the remember-forgotten comparison we in addition also discarded two additional units because these units fired no spikes during the presentation of the forgotten stimuli (making it impossible to estimate their SFC).

For time-frequency decompositions and phase-coherence analysis we used wavelets as implemented in the EEGLAB toolbox [74]. We used morlet wavelets composed of 3 cycles for time- frequency analysis and 1 cycle for phase-coherence analysis. For comparing the phase-coherence and power between remembered and forgotten images we also equalized

the number of trials. To exclude artifacts, trials during which the absolute value of the ECoG or field potentials exceeded 3x the s.d. were excluded.

Data and Software Availability

The spike detection and sorting toolbox OSort and the Chronux toolbox were used for data processing, both of which are available as open source. Data and custom MATLAB analysis scripts are available upon reasonable request.

Supplementary Material

Refer to Web version on PubMed Central for supplementary material.

Acknowledgments

References

1. Squire LR, Stark CEL, Clark RE. The medial temporal lobe. Annu Rev Neurosci. 2004; 27:279–306. [PubMed: 15217334]

2. Hansen N, Manahan-Vaughan D. Dopamine D1/D5 receptors mediate informational saliency that promotes persistent hippocampal long-term plasticity. Cereb Cortex. 2014; 24:845–858. [PubMed: 23183712]

3. Ito HT, Schuman EM. Frequency-dependent gating of synaptic transmission and plasticity by dopamine. Front Neural Circuits. 2007; 1:1. [PubMed: 18946543]

4. Gasbarri A, Sulli A, Packard MG. The dopaminergic mesencephalic projections to the hippocampal formation in the rat. Prog Neuropsychopharmacol Biol Psychiatry. 1997; 21:1–22. [PubMed: 9075256]

5. Adcock RA, Thangavel A, Whitfield-Gabrieli S, Knutson B, Gabrieli JDE. Reward-motivated learning: mesolimbic activation precedes memory formation. Neuron. 2006; 50:507–517. [PubMed: 16675403]

6. Wittmann BC, Schott BH, Guderian S, Frey JU, Heinze HJ, Düzel E. Reward-related FMRI activation of dopaminergic midbrain is associated with enhanced hippocampus-dependent long-term memory formation. Neuron. 2005; 45:459–467. [PubMed: 15694331]

7. Clausen B, Schachtman TR, Mark LT, Reinholdt M, Christoffersen GRJ. Impairments of exploration and memory after systemic or prelimbic D1-receptor antagonism in rats. Behav Brain Res. 2011; 223:241–254. [PubMed: 21497169]

8. Li S, Cullen WK, Anwyl R, Rowan MJ. Dopamine-depen-dent facilitation of LTP induction in hippocampal CA1 by exposure to spatial novelty. Nat Neurosci. 2003; 6:526–531. [PubMed: 12704392]

9. Lisman JE, Grace AA. The hippocampal-VTA loop: controlling the entry of information into long-term memory. Neuron. 2005; 46:703–713. [PubMed: 15924857]

10. Scimeca JM, Badre D. Striatal contributions to declarative memory retrieval. Neuron. 2012; 75:380–392. [PubMed: 22884322]

11. Chowdhury R, Guitart-Masip M, Bunzeck N, Dolan RJ, Düzel E. Dopamine modulates episodic memory persistence in old age. J Neurosci. 2012; 32:14193–14204. [PubMed: 23055489]

12. Schultz W. Dopamine reward prediction-error signalling: a two-component response. Nat Rev Neurosci. 2016; 17:183–195. [PubMed: 26865020]

13. Ljungberg T, Apicella P, Schultz W. Responses of monkey dopamine neurons during learning of behavioral reactions. J Neurophysiol. 1992; 67:145–163. [PubMed: 1552316]

14. Zaghloul KA, Blanco JA, Weidemann CT, McGill K, Jaggi JL, Baltuch GH, Kahana MJ. Human substantia nigra neurons encode unexpected financial rewards. Science. 2009; 323:1496–1499. [PubMed: 19286561]

15. Reynolds JNJ, Hyland BI, Wickens JR. A cellular mechanism of reward-related learning. Nature. 2001; 413:67–70. [PubMed: 11544526]

16. Mikell CB, Sheehy JP, Youngerman BE, McGovern RA, Wojtasiewicz TJ, Chan AK, Pullman SL, Yu Q, Goodman RR, Schevon CA, McKhann GM 2nd. Features and timing of the response of single neurons to novelty in the substantia nigra. Brain Res. 2014; 1542:79–84. [PubMed: 24161826]

17. McGovern RA, Chan AK, Mikell CB, Sheehy JP, Ferrera VP, McKhann GM 2nd. Human substantia nigra neurons encode decision outcome and are modulated by categorization uncertainty in an auditory categorization task. Physiol Rep. 2015; 3:e12422. [PubMed: 26416969]

18. Horvitz JC, Stewart T, Jacobs BL. Burst activity of ventral tegmental dopamine neurons is elicited by sensory stimuli in the awake cat. Brain Res. 1997; 759:251–258. [PubMed: 9221945]

19. Steinfels GF, Heym J, Strecker RE, Jacobs BL. Behavioral correlates of dopaminergic unit activity in freely moving cats. Brain Res. 1983; 258:217–228. [PubMed: 6824912]

20. Lak A, Stauffer WR, Schultz W. Dopamine neurons learn relative chosen value from probabilistic rewards. eLife. 2016; 5:e18044. [PubMed: 27787196]

21. Mai, JK., Paxinos, G., Voss, T. Atlas of the Human Brain. Third. Academic; 2008.

22. Miller KJ, Makeig S, Hebb AO, Rao RPN, denNijs M, Ojemann JG. Cortical electrode localization from X-rays and simple mapping for electrocorticographic research: the "Location on Cortex" (LOC) package for MATLAB. J Neurosci Methods. 2007; 162:303–308. [PubMed: 17343918]

23. Lisman J, Grace AA, Duzel E. A neoHebbian framework for episodic memory; roleof dopamine-dependent late LTP. Trends Neurosci. 2011; 34:536–547. [PubMed: 21851992]

24. Saitoh K, Isa T, Takakusaki K. Nigral GABAergic inhibition upon mesencephalic dopaminergic cell groups in rats. Eur J Neurosci. 2004; 19:2399–2409. [PubMed: 15128394]

25. Rutishauser U, Mamelak AN, Schuman EM. Single-trial learning of novel stimuli by individual neurons of the human hippocampus-amygdala complex. Neuron. 2006; 49:805–813. [PubMed: 16543129]

26. Rutishauser U, Ross IB, Mamelak AN, Schuman EM. Human memory strength is predicted by theta-frequency phase-locking of single neurons. Nature. 2010; 464:903–907. [PubMed: 20336071]

27. Antzoulatos EG, Miller EK. Increases in functional connectivity between prefrontal cortex and striatum during category learning. Neuron. 2014; 83:216–225. [PubMed: 24930701]

28. Backus AR, Schoffelen JM, Szebényi S, Hanslmayr S, Doeller CF. Hippocampal-prefrontal theta oscillations support memory integration. Curr Biol. 2016; 26:450–457. [PubMed: 26832442]

29. Fujisawa S, Buzsáki G. A4 Hz oscillation adaptively synchronizes prefrontal, VTA, and hippocampal activities. Neuron. 2011; 72:153–165. [PubMed: 21982376]

30. Kreiman G, Koch C, Fried I. Category-specific visual responses of single neurons in the human medial temporal lobe. Nat Neurosci. 2000; 3:946–953. [PubMed: 10966627]

31. Xiang JZ, Brown MW. Differential neuronal encoding of novelty, familiarity and recency in regions of the anterior temporal lobe. Neuropharmacology. 1998; 37:657–676. [PubMed: 9705004]

32. Faraut MCM, Carlson AA, Sullivan S, Tudusciuc O, Ross I, Reed CM, Chung JM, Mamelak AN, Rutishauser U. Dataset of human medial temporal lobe single neuron activity during declarative memory encoding and recognition. Sci Data. 2018; 5:180010. [PubMed: 29437158]

33. Rutishauser U, Ye S, Koroma M, Tudusciuc O, Ross IB, Chung JM, Mamelak AN. Representation of retrieval confidence by single neurons in the human medial temporal lobe. Nat Neurosci. 2015; 18:1041–1050. [PubMed: 26053402]

34. Loughlin SE, Fallon JH. Dopaminergic and non-dopaminergic projections to amygdala from substantia nigra and ventral tegmental area. Brain Res. 1983; 262:334–338. [PubMed: 6839161]

35. Francois C, Yelnik J, Tandé D, Agid Y, Hirsch EC. Dopaminergic cell group A8 in the monkey: anatomical organization and projections to the striatum. J Comp Neurol. 1999; 414:334–347. [PubMed: 10516600]

36. Beckstead RM, Domesick VB, Nauta WJH. Efferent connections of the substantia nigra and ventral tegmental area in the rat. Brain Res. 1979; 175:191–217. [PubMed: 314832]

37. Ison MJ, Mormann F, Cerf M, Koch C, Fried I, Quiroga RQ. Selectivity of pyramidal cells and interneurons in the human medial temporal lobe. J Neurophysiol. 2011; 106:1713–1721. [PubMed: 21715671]

38. Stauffer WR, Lak A, Yang A, Borel M, Paulsen O, Boyden ES, Schultz W. Dopamine neuron-specific optogenetic stimulation in rhesus macaques. Cell. 2016; 166:1564–1571e6. [PubMed: 27610576]

39. Ungless MA, Grace AA. Are you or aren't you? Challenges associated with physiologically identifying dopamine neurons. Trends Neurosci. 2012; 35:422–430. [PubMed: 22459161]

40. Hartigan JA, Hartigan PM. The dip test of unimodality. Ann Stat. 1985; 13:70–84.

41. Ramayya AG, Zaghloul KA, Weidemann CT, Baltuch GH, Kahana MJ. Electrophysiological evidence for functionally distinct neuronal populations in the human substantia nigra. Front Hum Neurosci. 2014; 8:655. [PubMed: 25249957]

42. Felten DL, Sladek JR Jr. Monoamine distribution in primate brain V. Monoaminergic nuclei: anatomy, pathways and local organization. Brain Res Bull. 1983; 10:171–284. [PubMed: 6839182]

43. Gerfen CR, Herkenham M, Thibault J. The neostriatal mosaic: II Patch- and matrix-directed mesostriatal dopaminergic and non-dopaminergic systems. J Neurosci. 1987; 7:3915–3934. [PubMed: 2891799]

44. Matsumoto M, Hikosaka O. Two types of dopamine neuron distinctly convey positive and negative motivational signals. Nature. 2009; 459:837–841. [PubMed: 19448610]

45. Joshua M, Adler A, Rosin B, Vaadia E, Bergman H. Encoding of probabilistic rewarding and aversive events by pallidal and nigral neurons. J Neurophysiol. 2009; 101:758–772. [PubMed: 19052110]

46. Fiorillo CD, Yun SR, Song MR. Diversity and homogeneity in responses of midbrain dopamine neurons. J Neurosci. 2013; 33:4693–4709. [PubMed: 23486943]

47. Richards CD, Shiroyama T, Kitai ST. Electrophysiological and immunocytochemical characterization of GABA and dopamine neurons in the substantia nigra of the rat. Neuroscience. 1997; 80:545–557. [PubMed: 9284356]

48. Damier P, Hirsch EC, Agid Y, Graybiel AM. The substantia nigra of the human brain. II Patterns of loss of dopamine-containing neurons in Parkinson's disease. Brain. 1999; 122:1437–1448. [PubMed: 10430830]

49. Fearnley JM, Lees AJ. Ageing and Parkinson's disease: substantia nigra regional selectivity. Brain. 1991; 114:2283–2301. [PubMed: 1933245]

50. Salgado S, Kaplitt MG. The nucleus accumbens: a comprehensive review. Stereotact Funct Neurosurg. 2015; 93:75–93. [PubMed: 25720819]

51. Hong S, Hikosaka O. Pedunculopontine tegmental nucleus neurons provide reward, sensorimotor, and alerting signals to midbrain dopamine neurons. Neuroscience. 2014; 282:139–155. [PubMed: 25058502]

52. Otani S, Bai J, Blot K. Dopaminergic modulation of synaptic plasticity in rat prefrontal neurons. Neurosci Bull. 2015; 31:183–190. [PubMed: 25822215]

53. Sheynikhovich D, Otani S, Arleo A. Dopaminergic control of long-term depression/long-term potentiation threshold in prefrontal cortex. J Neurosci. 2013; 33:13914–13926. [PubMed: 23966711]

54. Kramar CP, Chefer VI, Wise RA, Medina JH, Barbano MF. Dopamine in the dorsal hippocampus impairs the late consolidation of cocaine-associated memory. Neuropsychopharmacology. 2014; 39:1645–1653. [PubMed: 24442095]

55. Takeuchi T, Duszkiewicz AJ, Sonneborn A, Spooner PA, Yamasaki M, Watanabe M, Smith CC, Fernández G, Deisseroth K, Greene RW, Morris RG. Locus coeruleus and dopaminergic consolidation of everyday memory. Nature. 2016; 537:357–362. [PubMed: 27602521]

56. Schott BH, Minuzzi L, Krebs RM, Elmenhorst D, Lang M, Winz OH, Seidenbecher CI, Coenen HH, Heinze HJ, Zilles K, et al. Mesolimbic functional magnetic resonance imaging activations during reward anticipation correlate with reward-related ventral striatal dopamine release. J Neurosci. 2008; 28:14311–14319. [PubMed: 19109512]

57. Zavala B, Tan H, Ashkan K, Foltynie T, Limousin P, Zrinzo L, Zaghloul K, Brown P. Human subthalamic nucleus-medial frontal cortex theta phase coherence is involved in conflict and error related cortical monitoring. Neuroimage. 2016; 137:178–187. [PubMed: 27181763]

58. Kelley R, Flouty O, Emmons EB, Kim Y, Kingyon J, Wessel JR, Oya H, Greenlee JD, Narayanan NS. A human prefrontal-subthalamic circuit for cognitive control. Brain. 2018; 141:205–216. [PubMed: 29190362]

59. Nambu A, Tokuno H, Takada M. Functional significance of the cortico-subthalamo-pallidal 'hyperdirect' pathway. Neurosci Res. 2002; 43:111–117. [PubMed: 12067746]

60. Haber SN. The primate basal ganglia: parallel and integrative networks. J Chem Neuroanat. 2003; 26:317–330. [PubMed: 14729134]

61. Yoon JH, Minzenberg MJ, Raouf S, D'Esposito M, Carter CS. Impaired prefrontal-basal ganglia functional connectivity and substantia nigra hyperactivity in schizophrenia. Biol Psychiatry. 2013; 74:122–129. [PubMed: 23290498]

62. Tomasi D, Volkow ND. Functional connectivity of substantia nigra and ventral tegmental area: maturation during adolescence and effects of ADHD. Cereb Cortex. 2014; 24:935–944. [PubMed: 23242198]

63. Blumenfeld RS, Ranganath C. Prefrontal cortex and long-term memory encoding: an integrative review of findings from neuropsychology and neuroimaging. Neuroscientist. 2007; 13:280–291. [PubMed: 17519370]

64. Almeida L, Deeb W, Spears C, Opri E, Molina R, Martinez-Ramirez D, Gunduz A, Hess CW, Okun MS. Current practice and the future of deep brain stimulation therapy in Parkinson's disease. Semin Neurol. 2017; 37:205–214. [PubMed: 28511261]

65. Brainard DH. The Psychophysics Toolbox. Spat Vis. 1997; 10:433–436. [PubMed: 9176952]

66. Machado A, Rezai AR, Kopell BH, Gross RE, Sharan AD, Benabid AL. Deep brain stimulation for Parkinson's disease: surgical technique and perioperative management. Mov Disord. 2006; 21(Suppl 14):S247–S258. [PubMed: 16810722]

67. Lafreniere-Roula M, Hutchison WD, Lozano AM, Hodaie M, Dostrovsky JO. Microstimulation-induced inhibition as a tool to aid targeting the ventral border of the subthalamic nucleus. J Neurosurg. 2009; 111:724–728. [PubMed: 19408978]

68. Allison T. Localization of sensorimotor cortex in neurosurgery by recording of somatosensory evoked potentials. Yale J Biol Med. 1987; 60:143–150. [PubMed: 3577212]

69. Fischl B. FreeSurfer. Neuroimage. 2012; 62:774–781. [PubMed: 22248573]

70. Reuter M, Rosas HD, Fischl B. Highly accurate inverse consistent registration: a robust approach. Neuroimage. 2010; 53:1181–1196. [PubMed: 20637289]

71. Rutishauser U, Schuman EM, Mamelak AN. Online detection and sorting of extracellularly recorded action potentials in human medial temporal lobe recordings, in vivo. J Neurosci Methods. 2006; 154:204–224. [PubMed: 16488479]

72. Pouzat C, Mazor O, Laurent G. Using noise signature to optimize spike-sorting and to assess neuronal classification quality. J Neurosci Methods. 2002; 122:43–57. [PubMed: 12535763]

73. Harris KD, Henze DA, Csicsvari J, Hirase H, Buzsaáki G. Accuracy of tetrode spike separation as determined by simultaneous intracellular and extracellular measurements. J Neurophysiol. 2000; 84:401–414. [PubMed: 10899214]

74. Delorme A, Makeig S. EEGLAB: an open source toolbox for analysis of single-trial EEG dynamics including independent component analysis. J Neurosci Methods. 2004; 134:9–21. [PubMed: 15102499]

75. Maris E, Oostenveld R. Nonparametric statistical testing of EEG- and MEG-data. J Neurosci Methods. 2007; 164:177–190. [PubMed: 17517438]

76. Fries P, Reynolds JH, Rorie AE, Desimone R. Modulation of oscillatory neuronal synchronization by selective visual attention. Science. 2001; 291:1560–1563. [PubMed: 11222864]

77. Mitra, P., Bokil, H. Observed Brain Dynamics. Oxford University; 2007.

78. Vinck M, van Wingerden M, Womelsdorf T, Fries P, Pennartz CMA. The pairwise phase consistency: a bias-free measure of rhythmic neuronal synchronization. Neuroimage. 2010; 51:112–122. [PubMed: 20114076]

Highlights

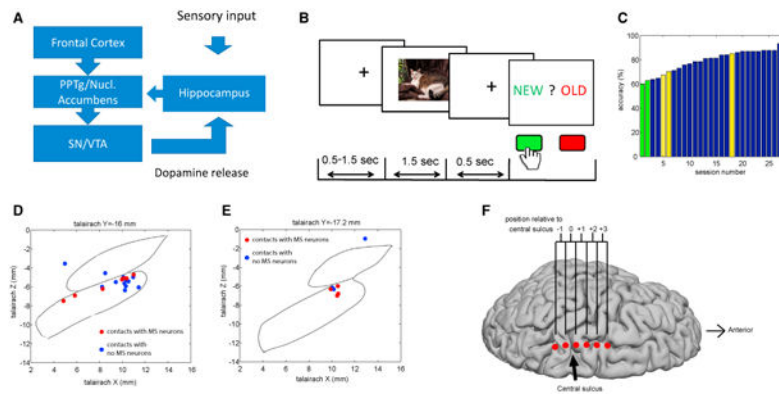- Human substantia nigra (SN) neurons are modulated by stimulus novelty

- Memory-selective neurons in substantia nigra are putatively dopaminergic

- Phase locking of SN neurons to frontal oscillations predicts memory formation

- Validates predictions of Lisman and Grace's VTA/SN-hippocampus loop model in humans

**Figure 1. Task, Behavior, and Recording Locations**

(A) Simplified summary of the Lisman-Grace model.

(B) The task. Top: screens presented to the subjects during an example trial. Bottom: the lengths of time for which each screen was shown.

(C) Behavior. Recognition accuracy of all sessions, rank ordered, is shown. Green bars indicate sessions with at-chance accuracy; yellow bars indicate sessions with recordings localized outside of SN.

(D and E) Location of microelectrode recording sites in Talairach space at $Y = -16$ (D) and $Y = -;17.2$ (E). Contours indicate atlas-derived borders of SN and STN [21]. A contact is colored in red if at least one memory selective neuron (see SN Neurons Differentiate between Novel and Familiar Stimuli and Cell Type Analysis) was recorded at this location and blue if otherwise.

(F) Location of cortical recordings. Shown is the median location of the recorded ECoG contacts across the six recording sessions for which an intraoperative X-ray image was available (see STAR Methods). See Figure S2D for an example from an individual subject. The reconstructed brain shown is a template brain [22].
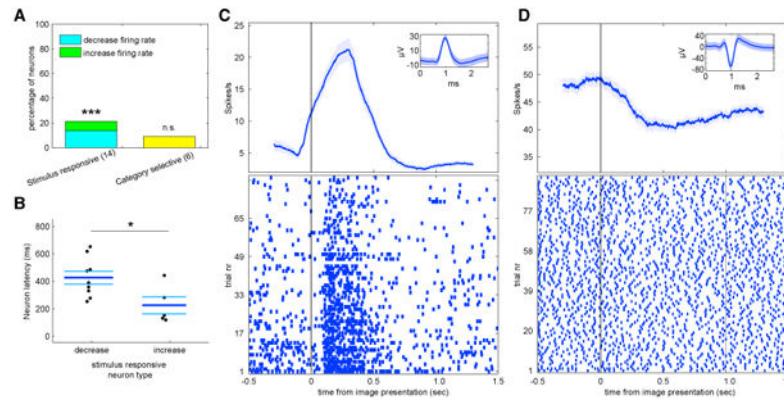
Figure 2. Image-Onset Responsive Neurons in the Human Substantia Nigra

(A) Percent of all recorded SN cells that responded to image presentation (left) or that were image category selective (right). The numbers below each comparison denote the numbers of neurons classified as each type. We tested whether the observed percentage was higher than that expected by chance by comparing with a null distribution estimated after scrambling the condition labels (repeated 500 times; *p < 0.05, **p < 0.01, and ***p 0.002).(B) Latency of neurons described in (A). Latency was defined as the first significant bin. Neurons that responded with an increase in firing rate responded significantly faster (p = 0.03). Each dot represents the response of one neuron. The three bars mark, from top to bottom, upper SEM, mean, and lower SEM.

(C and D) Two example cells that responded to image presentation with (C) an increase or (D) decrease in firing rate. Top: poststimulus time histograms (PSTHs) (bin size 400 ms; step size 1 ms). Shaded areas represent± SEM across trials. Image onset was at t = 0. Insets show the mean extracellular waveform ±SEM of all spikes that belong to this cell.
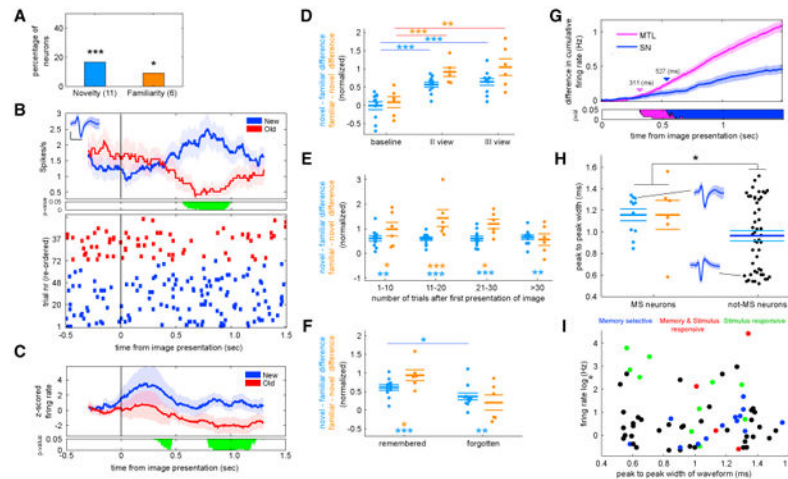
Figure 3. Memory Selective Neurons in the Human Substantia Nigra

(A) Percent of all recorded SN cells that showed a significant increase in firing rate to novel images (n = 11) or familiar images (n = 6; see also Figure S3).

(B) Example of a memory selective cell. Top: PSTH (bin size, 400 ms; step size,1 ms). Shaded areas represent ± SEM across trials. Middle: periods of significance marked in green (p < 0.05, permuted t test; corrected for multiple comparisons using a cluster-size correction). Bottom: raster plot with trials sorted according to image novelty/familiarity. The inset shows the mean extracellular waveform ± SEM of all spikes associated with this cell. Inset represents waveform of the neuron; vertical and horizontal scale bars mark 20 mV and 1 ms, respectively.

(C) Group PSTH of all units that increased their firing rate to novel images (n = 11). Shaded areas represent ± SEM across neurons. The bottom panel shows periods of significance (p < 0.05, permuted t test; corrected for multiple comparisons using a cluster-size correction; bin size 400 ms, step size 1 ms).

(D–F) Response of MS neurons as a function of the degree of familiarity and behavior. The metric used is the normalized difference in firing rate in response to novel and familiar images (see STAR Methods). Each dot represents one neuron. The three bars mark, from top to bottom, upper SEM, mean, and lower SEM. For (E) and (F), only the first repetition (familiar 1) was used.

(D) Responses differed significantly already the first time an image was repeated (familiar 1), with no further increases for the second repetition (familiar 2).

(E) Effects of number of trials that elapsed between the first (novel) and second (familiar) time an image was shown. The response was significantly different as early as 1–10 trials apart (p < 0.05), with no further significant change (p > 0.05).

(F) The difference in response between the first repetition and when the image was novel was significantly larger for novelty neurons when the patient correctly identified the image as familiar compared to when the patient forgot the image (p < 0.05).

(G) Latency analysis. Shown is the pairwise difference of the cumulative firing rate of all MS neurons in SN and medial temporal lobe between the preferred and non-preferred trial type (novel or familiar). Shaded areas represent ± SEM. The bottom panel shows periods of significance against zero in green (p < 0.05,permuted paired t test; corrected for multiple comparisons using a cluster-size correction).

(H) Comparison of extracellular spike waveform length between MS (left) and non-MS (right) neurons. The two waveforms shown are examples for the indicated data points. The waveform shown on the top is the same neuron that is shown in (B). MS neurons had significantly longer waveforms (t [65] = 2.65; p = 0.012; permuted t test). Each dot represents one neuron. The three bars mark, from top to bottom, upper SEM, mean, and lower SEM.

(I) Scatterplot of firing rate versus waveform with all recorded neurons. Average firing rate is computed during the entire experiment. * indicates p <0.05, ** indicates p < 0.01, and *** indicates p   0.002 for (A) and p   0.001 for rest. All pvalues are derived from non-parametric permutation tests (see STAR Methods).
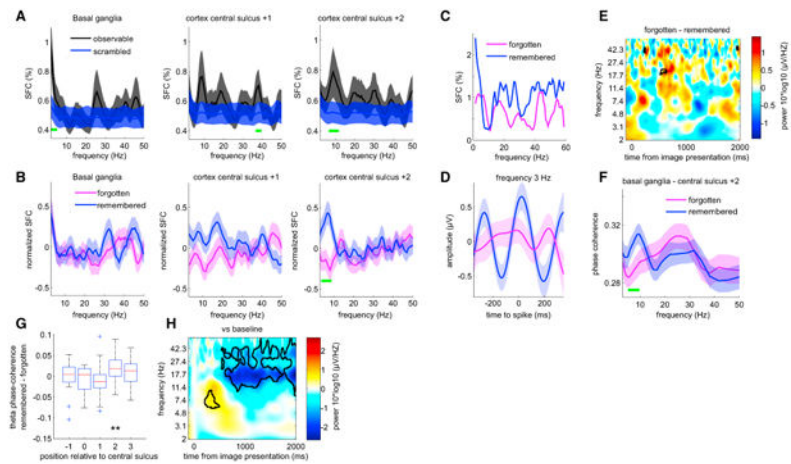
Figure 4. Substantia Nigra—Frontal Lobe Cortical Interactions Predict Success of Memory Encoding

(A) Average SFC of all SN neurons with field potential signals recorded in basal ganglia (left panel; n = 55 neurons) and cortex (middle and right panels; n = 61 neurons). SN neurons showed significant phase locking (marked in green) both locally (left panel) and to cortex (middle and right panel). Periods of significance relative to chance are marked in green (p < 0.05, corrected for multiple comparisons using a cluster-size correction; chance SFC shown in blue; estimated by randomly advancing spike times 500 times; see STAR Methods; see also Figure S4).

(B) Comparison of average SFC (as shown in A) between novel images that were later remembered (blue) or forgotten (magenta). Theta-band SFC with respect to central sulcus +2 was significantly larger in remembered compared to forgotten trials (right panel). The SFC was Z scored for each cell before averaging. Periods of significant differences are marked in green (p < 0.05, corrected for multiple comparisons using a cluster-size correction).

(C and D) Single-neuron example of SFC (C) and the spike triggered average (D), filtered in the 2–4 frequency band.

(E) Absence of theta-band power differences between remembered and forgotten novel trials in cortical ECoG (shown is central sulcus +2). Shown is a time frequency representation of the power difference between later forgotten and later remembered trials. Significant differences are marked by black contours (corrected for multiple comparisons using a cluster-size correction; see STAR Methods).

(F) Average phase coherence for all sessions as a function of frequency between basal ganglia field potentials and cortical ECoG signals recorded from the central sulcus +2 location. Periods of significant differences are marked in green (p < 0.05, corrected for multiple comparisons).

(G) The increased phase coherence in the theta band (5–10 Hz) between remembered and forgotten conditions was significant only in the central sulcus +2 pair.(H) Time frequency decomposition of cortical signals (central sulcus +2 pair) following image onset (t = 0). Significant differences relative to baseline are marked by black contours (corrected for multiple comparisons using a cluster-size correction; see STAR Methods). Beta power was significantly suppressed following image onset (color code represents differences versus baseline). In (A), (B), (D), and (F), shaded areas represent ± SEM. ** indicates p < 0.01.

Green bars indicate p < 0.05, corrected for multiple comparisons. All p values are derived from non-parametric permutation tests (see STAR Methods).